Supporting information

A molecular rotor-based turn-on sensor probe for amyloid fibrils in the extreme near-infrared region

1. Materials and Methods

Laser grade 1-ethyl-4-(4-(p-dimethylaminophenyl)-1,3-butadienyl)-quinolinumpercholate (styryl 11) was procured from Lambda Physik, and was used as received. Thioflavin-T (ultrapure grade) was obtained from Anaspec Inc and was used as received. Insulin (recombinant human) was obtained from Himedia Laboratories (India) whereas lysozyme (Hen egg white) was obtained from Sigma-Aldrich. Concentration of styryl-11 was determined from its optical density using its molar absorptivity ($\varepsilon \sim 14400\ M^{-1}cm^{-1}$ at 500 nm) in water.[1] All the measurements were carried out at ambient temperature, i.e. at $25\pm1^{o}C$.

A lyophilized powder of insulin (recombinant human insulin) was dissolved in pH 1.6 aqueous solution (using HCl), containing 100 mM NaCl, at a final insulin concentration of 2 mg/ml. The insulin solution was incubated at 65 °C for ~4 h, without mechanical agitation.[2] For emission measurements, the final concentration of styryl-11 was 15 μM at pH 7. The formation of insulin fibrils was confirmed by the Thioflavin-T (ThT) assay.

Lysozyme fibrils were prepared by following the method reported by Ahmed et. al.[3] Lysozyme (1.5 mg/mL) was dissolved in water and pH was maintained at 1.7 using HCl in the presence of 100 mM NaCl, and the solution was incubated at 65 °C with continuous stirring at 230 rpm. Fibril formation was confirmed by the ThT assay.

Ground-state absorption measurements were carried out on a Perkin Elmer UV/VIS spectrophotometer, model Lambda 25. Steady-state fluorescence measurements were performed on a Agilent Fluorescence spectrophotometer, model Cary Eclipse. For time-resolved fluorescence measurements, a diode-laser-based time-correlated single-photon counting (TCSPC) spectrometer (IBH, U.K.) was used, and has been described in detail elsewhere.[4] A 636 nm diode laser (1 MHz repetition rate) was used for the excitation of styryl-11 and a 406 nm diode laser for the excitation of Thioflavin-T. The fluorescence

transients were collected at the magic angle (54.7°) configuration. Magic angle collection ensures that the observed transient decays are not influenced by the rotational relaxation of the probe. The instrument response function (IRF) was measured by monitoring the scattered excitation light from the TiO_2 particles suspended in water. The measured IRF was ~120 ps.

The data analyzing software version DAS-6, from IBH, was used for the re-convolution analysis of the observed decays, following suitable exponential function, to obtain best fits for the decays. The quality of the fits and consequently the multi-exponential nature of the decays were judged by the reduced chi-square (χ^2) values and the distribution of the weighted residuals among the data channels. For a good fit, the χ^2 value is close to unity and the weighted residuals are distributed randomly around zero line among the data channels.

The decay traces are fitted with a multi-exponential function of the following form,[5]

$$I(t) = I(0)\sum \alpha_i \exp(-t/\tau_i) \quad (1)$$

The mean fluorescence lifetime is calculated according to the equation,[5]

$$<\tau>=\sum A_i\tau_i \text{ where } A_i = \alpha_i\tau_i / \sum \alpha_i\tau_i \quad (2)$$

Time-resolved fluorescence anisotropy measurements were carried out using the same TCSPC setup. In these measurements, polarized fluorescence decays, $I_{II}(t)$ and $I_{\perp}(t)$, with parallel and perpendicular emission polarizations, respectively, were recorded independently, exciting the samples with vertically polarized light source. The anisotropy decay function r(t) was subsequently constructed as[5]

$$r(t) = \frac{I_{II}(t) - GI_{\perp}(t)}{I_{II}(t) + 2GI_{\perp}(t)} \quad (3)$$

where, G is the correction factor for the polarization bias of the experimental set up. The G factor was independently estimated by measuring two perpendicularly polarized fluorescence decays, keeping the excitation light source horizontally polarized.

A Zeiss confocal fluorescence microscope setup (LSM 710) was used for obtaining the fluorescence images of the dyed insulin fibrils. Insulin fibrils were deposited on a glass slide surface. Before the deposition, the glass slide was cleaned by bath sonication by placing it in a vial containing iso-propanol/acetone/ethanol (2 min in each). The insulin fibril solution with styryl-11 was drop casted on top of the glass slide. A HeNe Laser (633 nm) source was used for the excitation of the sample whereas a 635 long pass filter was used on the emission side.

2. Docking calculation:

Molecular docking calculations are performed using AutoDock Vina.[6] The crystal structure of the fibrils was taken from the protein data bank (PDB IDs=2MXU,[7, 8] 5OQV,[9] and 2NAO[10]). For AutoDock software specific files, water molecules were removed and polar hydrogens were added whereas non-polar hydrogens were deleted and their charges were merged with the carbon atoms. An optimized structure of styryl-11 (using Gaussian 03), at the level of B3LYP, was then docked onto fibril using AutoDock Vina. The system was then investigated into a three dimensional volume of 80Å x 80Å x 80Å with a grid spacing of 1Å. The exhaustiveness parameter during docking calculation was set to 1000 to ensure a extensive search for the energetically best docked conformation. Discovery Studio Visualizer v16.1 software from Accelrys Software Inc. was used for visualization and schematic presentation of the docked conformations.

3. ***Binding constant for styryl-11-Fibril*:**

The binding constant of the styryl-11-fibril system was evaluated by fitting the data shown in the inset of figure 1A with the following equation

$$\frac{1}{F} = \frac{1}{F_{max}} + \frac{K_d}{F_{max}}\left(\frac{1}{C}\right) \quad (4)$$

where F is the fluorescence intensity, F_{max} is the maximal fluorescence intensity, K_d is the dissociation constant and C in the concentration of the protein.[11] This method was previously used to determine the dissociation constant of other amyloid markers with amyloid fibril.[2] The straight line fit (The plot of 1/F vs 1/C is in the insert of Figure 1A) resulted in a dissociation constant of $K_d = 2.1 \times 10^{-5}$ M.

4. ***Calculation of distance between ThT and Styryl-11 in fibril by FRET:***

The efficiency of Fluorescence Resonance Energy Transfer (FRET) between photoexcited ThT and styryl-11 was calculated using the following equation[5]

$$E = 1 - \frac{\langle \tau_{DA} \rangle}{\langle \tau_D \rangle} \quad (5)$$

The value of E was found to be 0.846 by considering the amplitude weighted lifetime of ThT in fibrillar solution in the presence and absence of styryl-11

The average separation between FRET pairs is given by following equation[5]

$$R = R_0 \sqrt[6]{\frac{1-E}{E}} \quad (6)$$

where, R_0, known as Forster distance and calculated by eq. 7

$$R_0 = 0.211[\kappa^2 n^{-4} Q_D J(\lambda)]^{1/6} \quad (7)$$

where, κ^2 is the orientation factor, which was assumed to be 2/3 for randomly oriented donor and acceptor, n (=1.4) is the refractive index for macromolecules in water, Q_D (=0.32) is the emission quantum yield of ThT in the fibrillar solution and J(λ) is overlap integral, which was calculated from the following equation.[5]

$$J(\lambda) = \frac{\int_0^\infty F_D(\lambda)\varepsilon_A(\lambda)\lambda^4 d\lambda}{\int_0^\infty F_D(\lambda) d\lambda} \quad (8)$$

where, ε_A is extinction coefficient of the acceptor (styryl-11), F_D is fluorescence intensity of donor

The value of R_0 was calculated using eq. 7 and 8 and was found to be 44.2Å. Using this value of R_0, the value of R was calculated using eq. 6 and was found to be 33.3 Å.

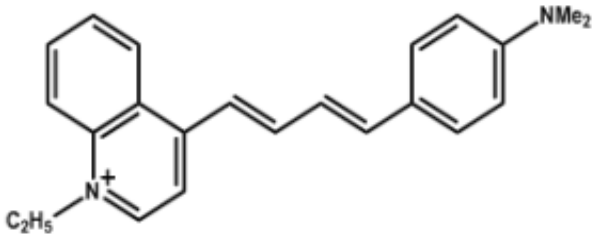

Scheme S1: Chemical structure of styryl-11

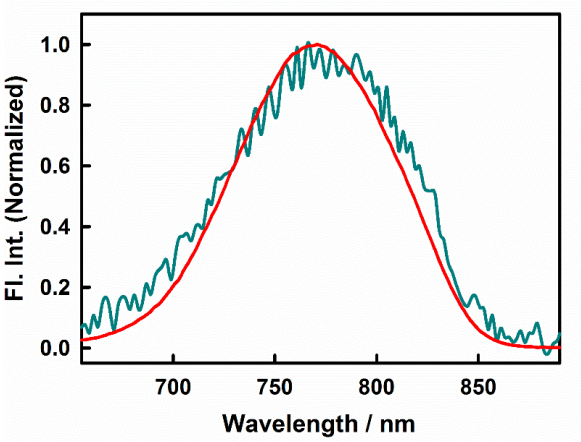

Figure S1. Normalized steady-state fluorescence spectra of styryl-11 in water (turquoise) and styryl-11 in 30µM Insulin fibril.

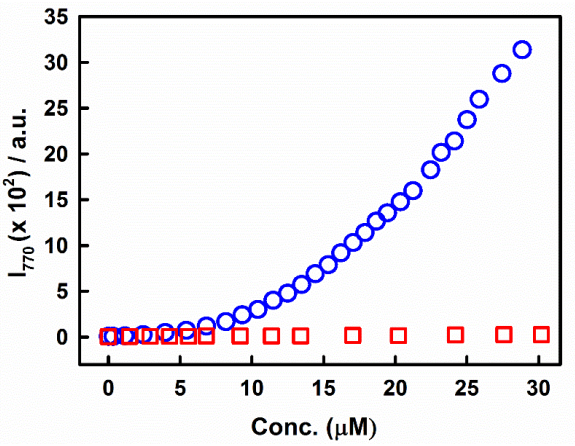

Figure S2. The blue circles represent the data points of steady-state fluorescence (λ_{ex} = 630 nm, λ_{em} = 770 nm) monitored for titration of styryl-11 against insulin fibril whereas the red squares represent that for titration of styryl-11 against native Insulin protein.

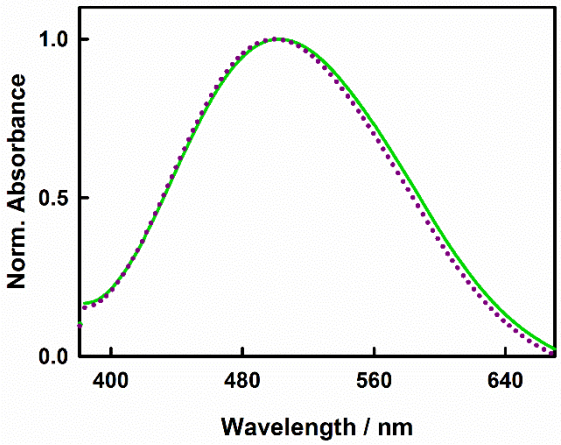

Figure S3. Normalized absorption spectra of styryl-11 in water (dotted dark red) and styryl-11 in presence of 30μM native Insulin (green).

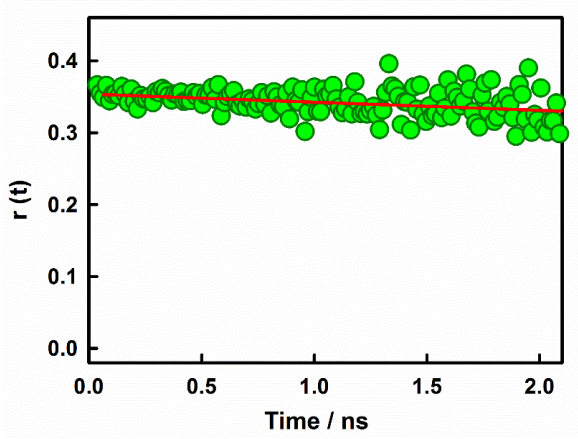

Figure S4. The filled green circles represent the data points for fluorescence anisotropy decay trace (λ_{ex} = 636 nm, λ_{em} = 770 nm) of styryl-11 in presence of 30μM Insulin fibril. The red solid line represents the fitting according to the exponential decay model.

Figure S4 shows that there is an insignificant temporal decrease in the anisotropy value and a large value of residual anisotropy which can be assigned to a strong immobilization of the probe in the fibril medium. Note that the rotational relaxation time of the free probe in the aqueous medium could not be directly measured due to its short lifetime, but is expected to be ~50 ps, considering its molecular dimensions. Thus, such a drastic increase in the rotational correlation time of the probe suggests a strong immobilization of the probe in the amyloid fibril medium, which is also consistent with the large increase in emission intensity and excited-state lifetime of the amyloid bound probe.

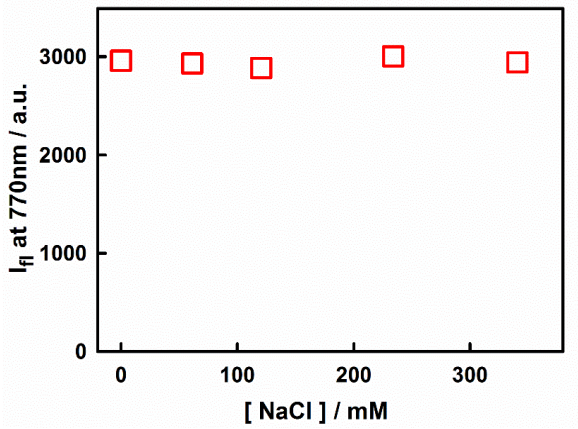

Figure S5: Variation of emission intensity at 770nm (λ_{ex} = 630 nm) with increasing concentration of NaCl in a solution containing styryl-11-fibril complex.

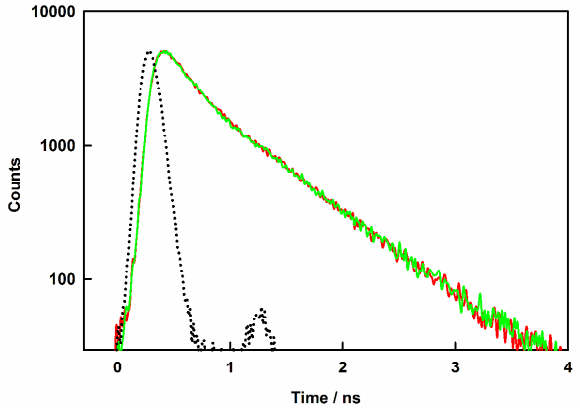

Figure S6. Transient emission decay trace (λ_{ex} = 636 nm, λ_{em} = 770 nm) of styryl-11-fibril complex in presence of 330 mM NaCl (in red) as well as in the absence of NaCl (in green). IRF is represented by black-dotted line.

The ionic strength dependent results, obtained in the present case, are in sharp contrast to the most widely used cationic amyloid probe, thioflavin-T, where the emission yield of the ThT-fibril complex is reported to be highly sensitive to the ionic strength of the medium.

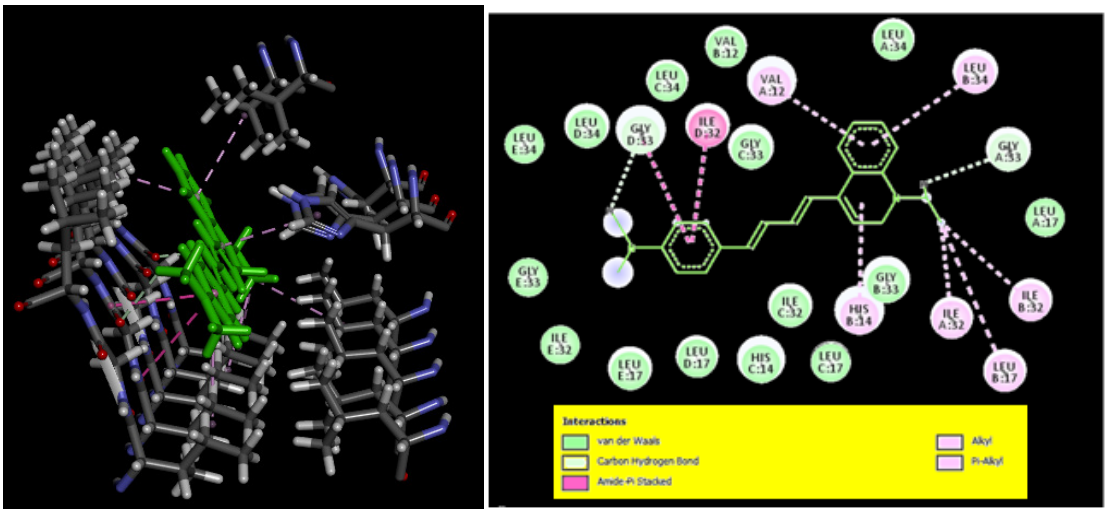

Figure S7: Left panel: Representation of the interaction pocket of the fibril showing different types of interactions operative in the styryl-11–fibril complex (styryl-11 is shown as stick model colored in green and the pocket amino acids are shown as sticks). **Right Panel**: Two-dimensional schematic diagram representing interactions between styryl-11 and neighboring residues of fibril.

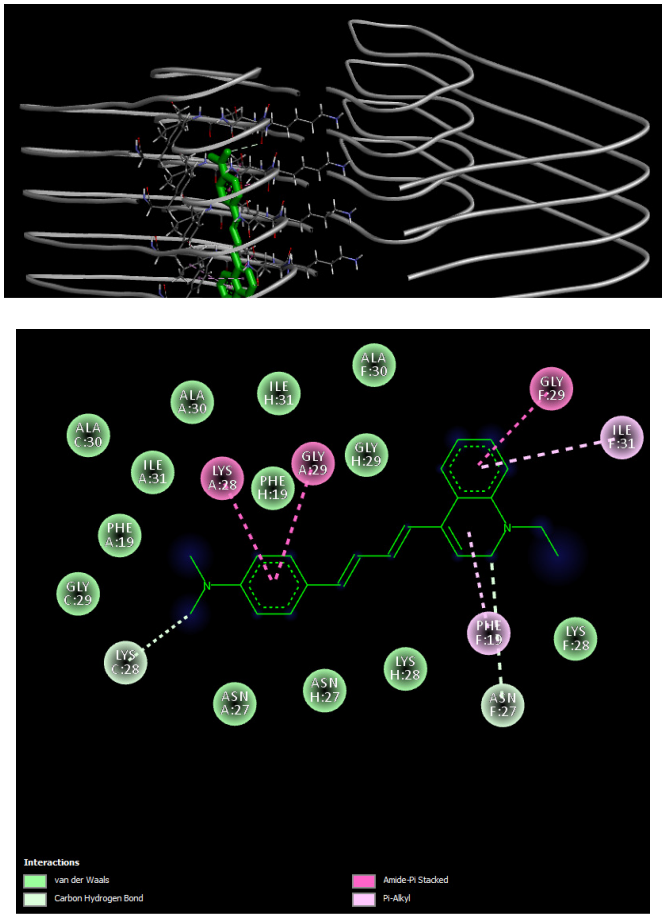

Figure S8: (Top): Molecular docking diagram showing the location of the binding site of the styryl-11 Aβ fibril (PDB ID = 5OQV) Bottom: Two-dimensional schematic diagram representing interactions between styryl-11 and neighboring residues of fibril

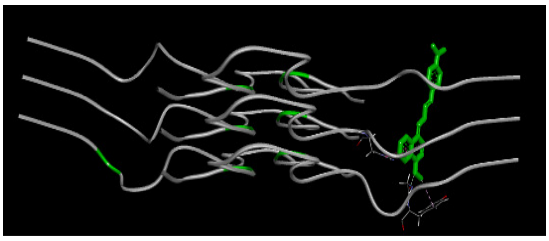

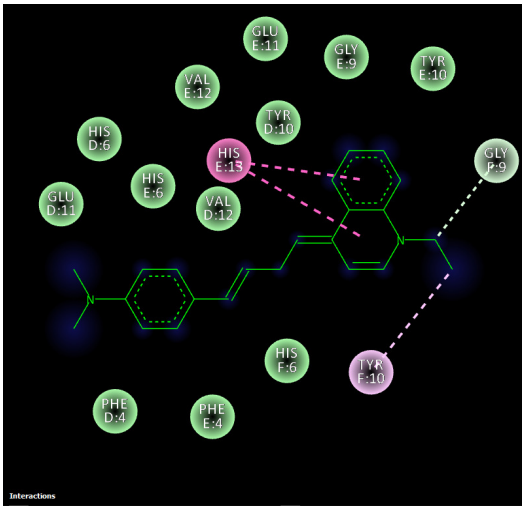

Figure S9: (Top): Molecular docking diagram showing the location of the binding site of the styryl-11 Aβ fibril (PDB ID = 2NAO) Bottom: Two-dimensional schematic diagram representing interactions between styryl-11 and neighboring residues of fibril

Although, slight variation in the docking results may appear due to the difference in amino acid sequence between insulin protein and amyloid beta protein, the current docking results provide a gross overview of the binding mode of styryl-11 to a representative beta sheet structure.

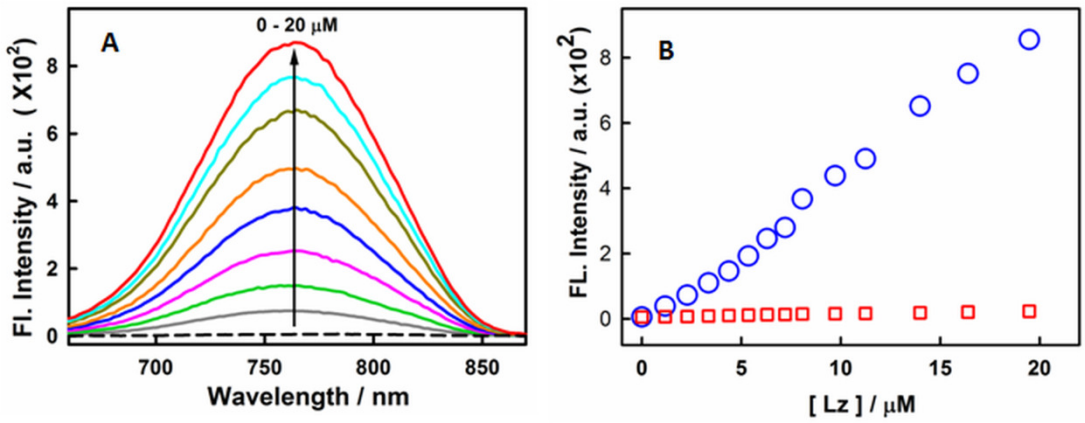

Figure S10: (A) Fluorescence spectra of 15 μM styryl-11 with the increasing concentration of lysozyme fibrils (0-20 μM) [λ_{ex} = 630 nm] (B) The blue circles represent the data points of steady-state fluorescence (λ_{ex} = 630 nm, λ_{em} = 770 nm) monitored for titration of styryl-11 against lysozyme fibril whereas the red squares represent that for titration of styryl-11 against native lysozyme protein.

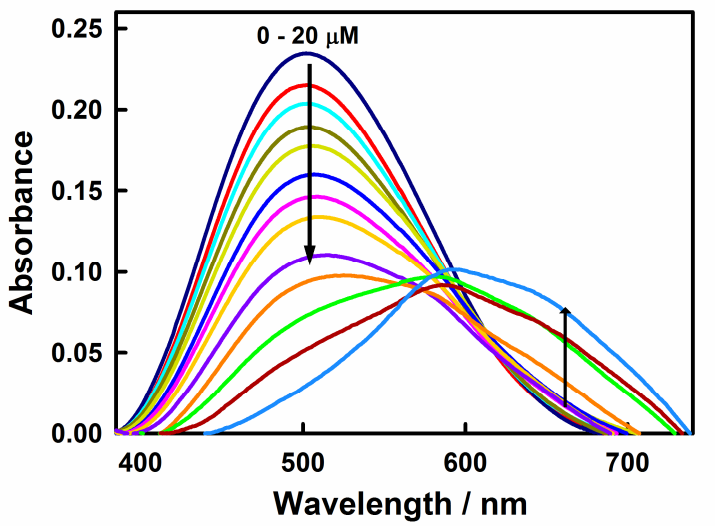

Figure S11: Absorption spectra of 15 μM styryl-11 with the increase in concentration of lysozyme fibrils (0-20 μM).

Competitive binding and energy transfer experiments

Thus, to gain an idea about the binding location of the styryl-11 in the fibrillar medium, we carried out competitive binding experiments with the well-established amyloid marker Thioflavin-T. Figure S7 presents the results of these experiments when ThT is added to a styryl-fibril complex.

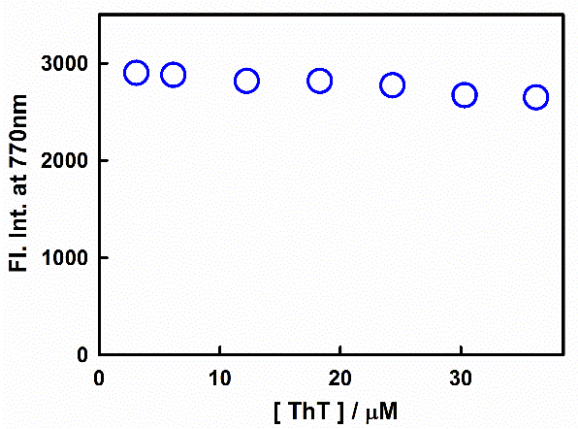

Figure S12: Variation of emission intensity at 770nm (λ_{ex} = 630 nm) with increasing concentration of ThT in a solution containing styryl-11-fibril complex.

It is quite evident that the emission features of the styryl-fibril complex remain completely unchanged with the addition of varying amount of ThT in the solution. These results were further supported by time-resolved emission measurements (Figure S8).

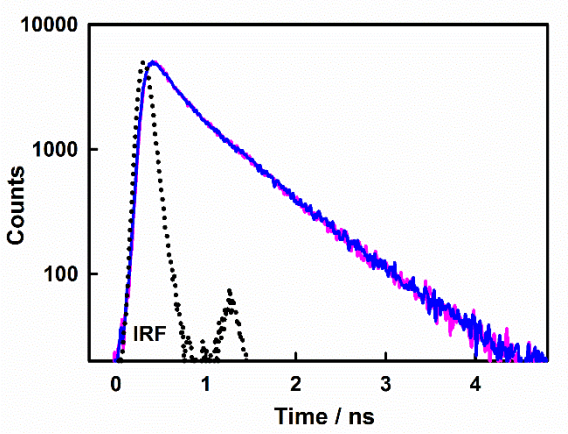

Figure S13. Transient emission decay trace (λ_{ex} = 636 nm, λ_{em} = 770 nm) of styryl-fibril complex in presence of 30μM ThT (in pink) as well as in the absence of ThT (in blue). IRF is represented by black-dotted line.

Thus, it clearly suggests that ThT and styryl-11 dye does not share a common binding site on the insulin fibril. However, we realized that there is a reasonable extent of spectral overlap that exists between the emission spectrum of the fibril bound ThT and the absorption spectra of the styryl-11, thus, we attempted to inspect any energy transfer taking place between them in the fibrillar medium when ThT is treated as a donor and the styryl-11 as an acceptor so that an idea about the mutual distance between the two dyes in the amyloid matrix can be obtained.

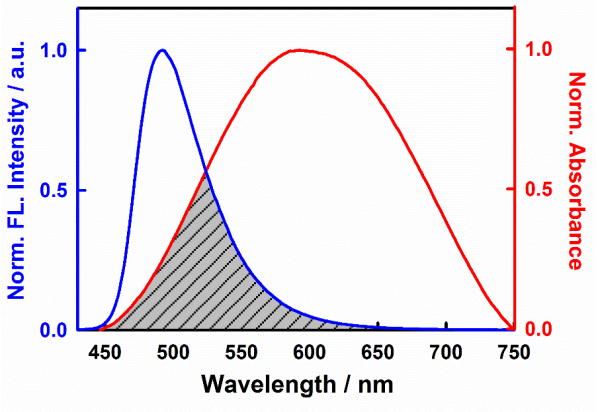

Figure S14: Normalized emission spectra of ThT-Fibril complex (solid blue line) and normalized absorption spectra of styryl-11-Fibril complex (solid red line) representing the overlapping area shown by grey shaded region.

For this purpose, we gradually added styryl-11 to a solution of ThT-fibril complex, with the excitation wavelength set for Thioflavin-T, and the results have been presented in Figure S10. It can be seen from figure S10A that, the emission of the ThT-fibril complex gradually decreases with gradual addition of styryl-11 in the solution. Interestingly, a new emission band appears at ~770 nm which corresponds to the emission of the styryl-11 dye. Thus, this decrease in the ThT emission (donor) and increase in the styryl-11 emission (acceptor) is a clear indication of the energy transfer taking place between the two dyes in the fibrillar medium.

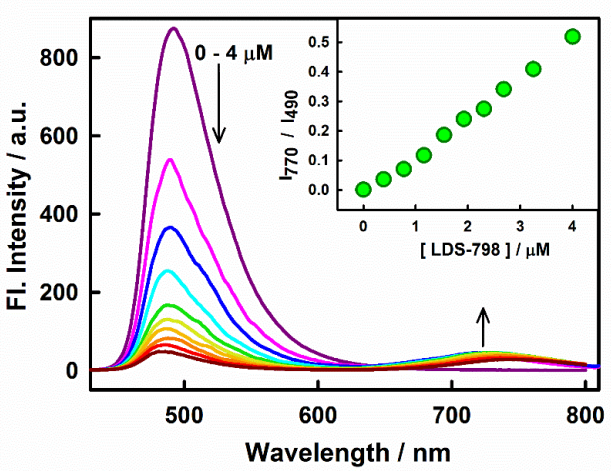

Figure S15 Fluorescence spectra of ThT-Fibril system with increasing concentration of styryl-11 (λ_{ex} = 440 nm). Inset shows the change in the ratio of fluorescence intensity at 770 nm (corresponding to styryl-11 emission) and 490 nm (corresponding to ThT emission) with increasing concentration of styryl-11.

To ensure that the emission at 770 nm does not arise from the direct excitation of the acceptor at the donor excitation wavelength, we have also performed a blank measurement of the same solution minus the donor (ThT), and we donot see any emission at 770 nm, thus confirming the origin of emission at 770 nm due to energy transfer (Figure S11).

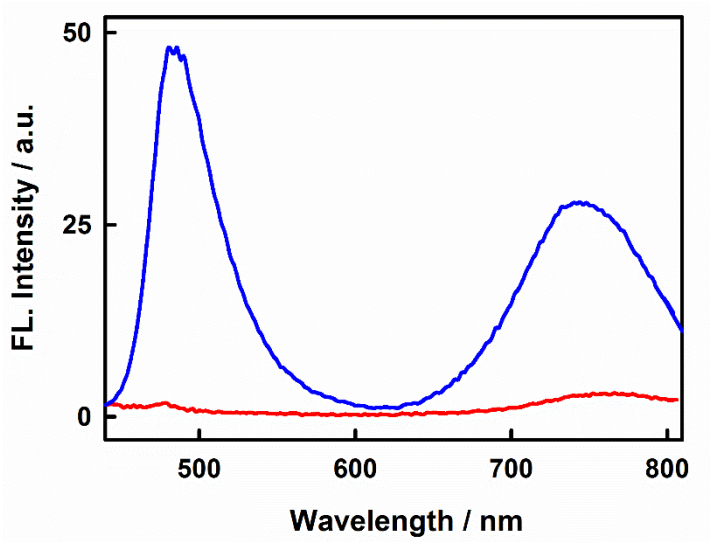

Figure S16. Emission spectra (λ_{ex} = 410 nm) monitored for styryl-11 (4μM) bound to ThT-fibril complex (blue) and styryl-11 bound to the same concentration of fibril (18μM) in absence of ThT (red).

The phenomenon of energy transfer was further validated by excitation spectra when the emission was monitored at 770 nm (Figure S9, ESI). Apart from a peak at 630 nm, corresponding to styryl-11, the excitation spectrum shows a dominant peak at 440 nm. The peak at 440 nm is characteristic of the excitation spectra of ThT-fibril complex. Thus, the appearance of the dominant ThT peak in the excitation spectra while monitoring emission at

770 nm, clearly suggests that the emission at 770 nm originates from ThT due to energy transfer.

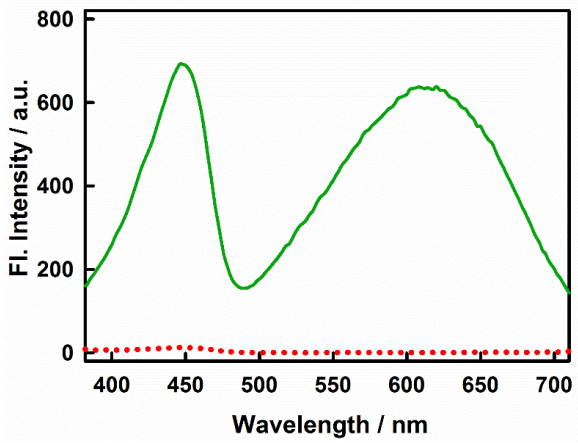

Figure S17: Excitation spectra (λ_{em} = 740 nm) monitored for styryl-11 (2 μM) bound to ThT-fibril complex (green) and ThT-fibril complex in absence of styryl-11 (dotted red).

The phenomenon of energy transfer was also investigated by time-resolved emission measurements and figure S13 summarizes the results of these measurements.

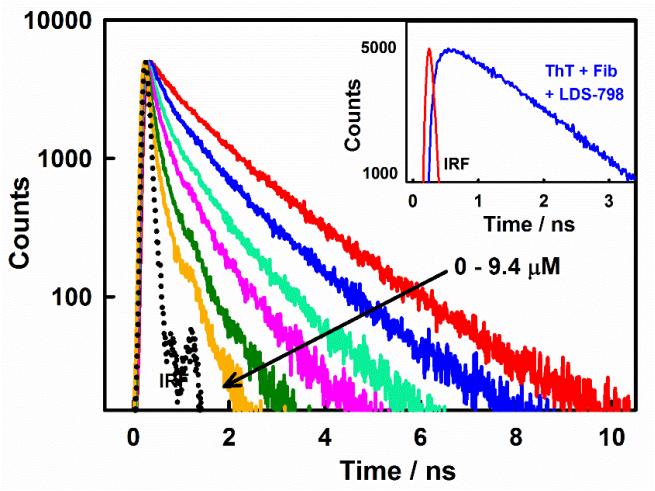

Figure S18: Fluorescence decay traces for ThT-Fibril system [λ_{ex} = 406 nm and λ_{em} = 490 nm] with increasing concentration of styryl-11 (0 -9.4 μM). Inset shows the transients, monitored at 770 nm, corresponding to styryl-11 emission with excitation centred at ThT (406 nm)

As evident from the figure, the transient decay trace for the ThT (donor) in the fibril matrix gradually becomes faster with gradual addition of styryl-11 (acceptor) which is a common

characteristic of the energy transfer phenomenon. However, from the acceptor's perspective, the rising component in the transient decay trace, when emission is monitored at the acceptor emission wavelength, provides another strong evidence for energy transfer phenomenon. The inset of Figure S10 B clearly shows a rise component in the transient decay trace when it is monitored at 770 nm, for ThT-fibril-Stryl-11 system, while the rise component is absent when ThT is not present in the system, clearly attesting the phenomenon of energy transfer in the present system. Using this phenomenon of energy transfer, the distance between the ThT and the styryl-11 was calculated to be 33.2 Å.

Table T1: Comparison of various fluorescent probes for sensing amyloid fibril

Sensing probe	**Species detected**	**K_d**	**Emission wavelength (nm)**	**Fold increase**	**Reference**
Styryl-11	Insulin fibrils	**20 μM**	**770**	**500**	**Current work**
Thioflavin-T	Insulin fibrils	10.4 μM	490	400	**Ref 12**
Auramine-O	Insulin fibrils	1.12 μM	560	<100	**Ref 2, 13**
1-Amino Napthalene dulfonate (ANS)	Insulin fibrils	2.3 μM	505		**Ref 14**
1,2-bis[4-(3-sulfonatopropoxyl)phenyl]-1,2-diphenylethene (BSPOTPE)	Insulin fibrils	10 μM	470	60	**Ref 15**
Luminescent conjugated polythiophene derivates (LCPs)	Insulin fibrils	0.2-2.4 μM	555-573	<100	**Ref 16**
Amino naphthalenyl-2-cyano-acrylate (ANCA) derivatives	Insulin fibrils	1.4-13.8 μM	535-550	6.5-8.5	**Ref 17**
Nile red	Insulin fibrils	12 μM	650	31	**Ref 18**

Stilbene derivative	$A\beta_{40}$ fibrils	1.13 μM	440	25	**Ref 19**
Curcumin derivative	$A\beta_{40}$ fibrils	105.8 nM	672	91.9	**Ref 20**
Thiophene derivative	$A\beta_{40}$ fibrils	10 nM	612	400	**Ref 21**
Alkatriene derivative	$A\beta_{40}$ fibrils	106 nM	685	26	**Ref 22**

Acknowledgement: The authors gratefully acknowledge the help from Dr. M. Kumbhakar, BARC for his help in collecting the fluorescence microscopic images, and Prof. A. Datta, IIT Powai for his help in quantum chemical calculations.

References

1 P. Sarkar, R. Luchowski, S. Raut, N. Sabnis, A. Remaley, A. G. Lacko, S. Thamake, Z. Gryczynski, and I. Gryczynski, *Biophys. Chem.*, 2010, **153**, 61.

2 N. Amdursky and D. Huppert, *J. Phys. Chem. B*, 2012, **116**, 13389−13395.

3 S. A. Muthu, N. Mothi, S. M. Shiriskar, R. R. S. Pissurlenkar, A. Kumar, and B. Ahmad, *Archives of Biochemistry and Biophysics*, 2016, **592**, 10.

4 M. Sayed, M. Sundararajan, J. Mohanty, A. C. Bhasikuttan, and H. Pal, *J. Phys. Chem. B*, 2015, **119**, 3046−3057.

5 J. R. Lakowicz, 'Principle of Fluorescence Spectroscopy', Plenum Press, 2006.

6 O. Trott and A. J. Olson, *J. Comput. Chem.*, 2010, **31**, 455−461.

7 G.-Q. Gao and A.-W. Xu, *RSC Adv.*, 2013, **3**, 21092.

8 Y. Xiao, B. Ma, D. McElheny, S. Parthasarathy, F. Long, M. Hoshi, R. Nussinov, and Y. Ishii, *Nat. Struct. Mol. Biol.*, 2015, **22**, 499.

9 L. Gremer, D. Scholzel, C. Schenk, E. Reinartz, J. Labahn, R. B. G. Ravelli, M. Tusche, C. Lopez-Iglesias, W. Hoyer, H. Heise, D. Willbold, and G. F. Schroder, *Science*, 2017, **358**, 116.

10 M. A. Walti, F. Ravotti, H. Arai, C. G. Glabe, J. S. Wall, A. Bockmann, P. Guntert, B. H. Meier, and R. Riek, *Proc. Natl. Acad. Sci. USA*, 2016, **113**, E4976.

11 J. L. Wang and G. M. Edelman, *J. Biol. Chem.*, 1971, **246**, 1185−1191.

[12] M. Groenning, M. Norrman, J. M. Flink, M. v. d. Weert, J. T. Bukrinsky, G. Schluckebier, and S. Frokjaer, *J. Struct. Biol.*, 2007, **159**, 483.

[13] N. H. Mudliar, B. Sadhu, A. M. Pettiwala, and P. K. Singh, *J. Phys. Chem. B*, 2016, **120**, 10496−10507.

[14] K. M. Psonka-Antonczyk, J. Duboisset, B. T. Stokke, T. Zako, T. Kobayashi, M. Maeda, S. Nyström, J. Mason, P. Hammarström, K. P. R. Nilsson, and M. Lindgren, *Int. J. Mol. Sci.*, 2012, **13**, 1461.

[15] Y. Hong, L. Meng, S. Chen, C. W. T. Leung, L.-T. Da, M. Faisal, D.-A. Silva, J. Liu, J. W. Y. Lam, X. Huang, and B. Z. Tang, *J. Am. Chem.Soc.*, 2012, **134**, 1680−1689.

[16] A. Åslund, A. Herland, P. Hammarström, K. P. R. Nilsson, B.-H. Jonsson, O. Inganäs, and P. Konradsson, *Bioconjugate Chem.*, 2007, **18**, 1860.

[17] W. M. Chang, M. Dakanali, C. C. Capule, C. J. Sigurdson, J. Yang, and E. A. Theodorakis, *ACS Chem Neurosci*, 2011, **2**, 249−255.

[18] R. Mishra, D. Sjolander, and P. Hammarstrom, *Mol. BioSyst.*, 2011, **7**, 1232.

[19] M. C. Hong, Y. K. Kim, J. Y. Choi, S. Q. Yang, H. Rhee, Y. H. Ryu, and e. al., *Bioorg Med Chem.*, 2010, **18**, 7724−7730.

[20] X. L. Zhang, Y. L. Tian, Z. Li, X. Y. Tian, H. B. Sun, and H. e. a. Liu, *J Am Chem Soc*, 2013, **135**, 16397.

[21] E. E. Nesterov, J. Skoch, B. T. Hyman, W. E. Klunk, B. J. Bacskai, and T. M. Swager, *Angew. Chem. Int. Ed.* , 2005, **44**, 5452

[22] H. Fu, M. Cui, P. Tu, Z. Pan, and B. Liu, *Chem Commun*, 2014, **50**, 11875−11878.